Article

Cell Reports

# A Sequentially Priming Phosphorylation Cascade Activates the Gliomagenic Transcription Factor Olig2

## Graphical Abstract

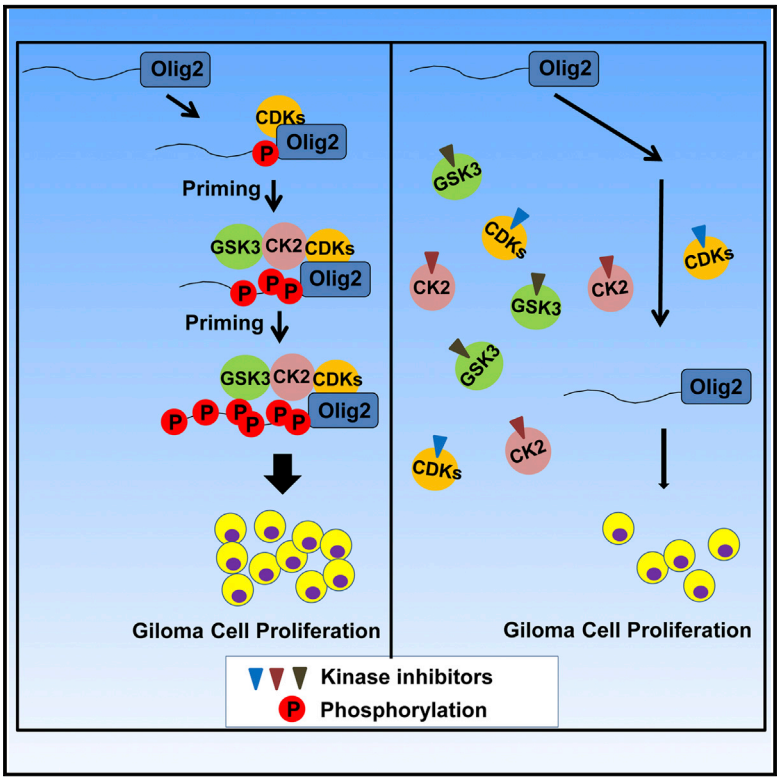


## Highlights

- OLIG2 promotes mitosis of normal and malignant neural progenitor cells
- These OLIG2 functions are contingent upon phosphorylation of a triple serine motif
- Kinases that phosphorylate this motif were identified as GSK3α/β, CK2, and CDK1/2
- Small inhibitors of the OLIG2 kinases can suppress gliomagenic functions of OLIG2

## Authors

Jing Zhou, An-Chi Tien, John A. Alberta, ..., Jarrod A. Marto, David H. Rowitch, Charles D. Stiles

## Correspondence

rowitchd@peds.ucsf.edu (D.H.R.), charles_stiles@dfci.harvard.edu (C.D.S.)

## In Brief

The transcription factor OLIG2 promotes mitosis of normal and malignant neural progenitor cells. Zhou et al. have identified a set of protein kinases that are both necessary and sufficient to phosphorylate a key regulatory triple serine motif in OLIG2. Small inhibitors of these kinases suppress gliomagenic functions of OLIG2.

Zhou et al., 2017, Cell Reports *18*, 3167–3177
March 28, 2017 
http://dx.doi.org/10.1016/j.celrep.2017.03.003

CellPress

Cell Reports
Article



# A Sequentially Priming Phosphorylation Cascade Activates the Gliomagenic Transcription Factor Olig2

Jing Zhou,[1,2,13] An-Chi Tien,[3,13] John A. Alberta,[1,2] Scott B. Ficarro,[2,4,5] Amelie Griveau,[3] Yu Sun,[1,2] Janhavee S. Deshpande,[2] Joseph D. Card,[2] Meghan Morgan-Smith,[6] Wojciech Michowski,[2,7] Rintaro Hashizume,[8] C. David James,[8] Keith L. Ligon,[9,10] William D. Snider,[6] Peter Sicinski,[2,7] Jarrod A. Marto,[2,5,9,10] David H. Rowitch,[3,11,12,*] and Charles D. Stiles[1,2,14,*]

[1]Department of Neurobiology, Harvard Medical School, Boston, MA 02115, USA
[2]Department of Cancer Biology, Dana-Farber Cancer Institute, Boston, MA 02215, USA
[3]Departments of Pediatrics and Neurosurgery, University of California, San Francisco, 35 Medical Center Way, San Francisco, CA 94143, USA
[4]Department of Biological Chemistry and Molecular Pharmacology, Harvard Medical School, Boston, MA 02115, USA
[5]Blais Proteomics Center, Dana-Farber Cancer Institute, Boston, MA 02215, USA
[6]UNC Neuroscience Center, University of North Carolina, Chapel Hill, NC 27599, USA
[7]Department of Genetics, Harvard Medical School, Boston, MA 02115, USA
[8]Department of Neurological Surgery, Northwestern University Feinberg School of Medicine, 300 E. Superior, Chicago, IL 60611, USA
[9]Department of Oncologic Pathology, Dana-Farber Cancer Institute, Boston, MA 02215, USA
[10]Department of Pathology, Brigham and Women's Hospital and Harvard Medical School, Boston, MA 02115, USA
[11]Eli and Edythe Broad Center of Regeneration Medicine and Stem Cell Research, University of California, San Francisco, 35 Medical Center Way, San Francisco, CA 94143, USA
[12]Department of Pediatrics, University of Cambridge, Wellcome Trust-MRC Cambridge Stem Cell Institute, Cambridge CB2 0AH, UK
[13]Co-first author
[14]Lead Contact
*Correspondence: rowitchd@peds.ucsf.edu (D.H.R.), charles_stiles@dfci.harvard.edu (C.D.S.)
http://dx.doi.org/10.1016/j.celrep.2017.03.003

## SUMMARY

**During development of the vertebrate CNS, the basic helix-loop-helix (bHLH) transcription factor Olig2 sustains replication competence of progenitor cells that give rise to neurons and oligodendrocytes. A pathological counterpart of this developmental function is seen in human glioma, wherein Olig2 is required for maintenance of stem-like cells that drive tumor growth. The mitogenic/gliomagenic functions of Olig2 are regulated by phosphorylation of a triple serine motif (S10, S13, and S14) in the amino terminus. Here, we identify a set of three serine/threonine protein kinases (glycogen synthase kinase 3α/β [GSK3α/β], casein kinase 2 [CK2], and cyclin-dependent kinases 1/2 [CDK1/2]) that are, collectively, both necessary and sufficient to phosphorylate the triple serine motif. We show that phosphorylation of the motif itself serves as a template to prime phosphorylation of additional serines and creates a highly charged "acid blob" in the amino terminus of Olig2. Finally, we show that small molecule inhibitors of this forward-feeding phosphorylation cascade have potential as glioma therapeutics.**

## INTRODUCTION

A pivotal development in vertebrate evolution was the appearance of myelinating oligodendrocytes that enwrap neural axons in the CNS. By enabling saltatory conductivity of electrical impulses, oligodendrocytes enabled the vertebrate brain to grow large and complex. During CNS development, the basic helix-loop-helix (bHLH) transcription factor Olig2 plays two essential roles in the formation of oligodendrocytes throughout the CNS. At late stages of CNS development, Olig2 instructs neural progenitors to exit the cell cycle and adopt an oligodendrocyte fate. However, at earlier stages of development, Olig2 actually opposes cell cycle exit and sustains replication competence so as to allow an adequate pool of oligodendrocyte progenitors to accumulate (Meijer et al., 2012).

Unfortunately, there is a pathological counterpart of this second function. Tumor-initiating cells with stem-like properties have been isolated from a wide range of adult and pediatric astrocytomas (Galli et al., 2004; Hemmati et al., 2003; Ignatova et al., 2002; Singh et al., 2003). Irrespective of patient age or tumor grade, these stem-like cells are marked by Olig2 (Bouvier et al., 2003; Ligon et al., 2004, 2007; Lu et al., 2001; Marie et al., 2001; Ohnishi et al., 2003). Beyond merely marking these stem-like cells, Olig2 is required for maintenance of the stem-like state and is essential for tumor formation from intracranial xenografts of human glioblastomas (Ligon et al., 2007; Mehta et al., 2011; Suvà et al., 2014). To a large extent, the gliomagenic

functions of Olig2 reflect an oppositional relationship with p53 functions (Mehta et al., 2011). Although p53 signaling is the most frequently mutated signaling axis in glioblastoma, the majority of glioblastomas retain at least one intact copy of the p53 gene (Cancer Genome Atlas Research Network, 2008). Complete ablation of p53 in human gliomas or genetically relevant murine models of glioma eliminates the tumorigenic requirement for Olig2 (Mehta et al., 2011).

Several years ago, we showed that the mitogenic function of Olig2 in normal oligodendrocyte progenitors and the anti-p53 functions of Olig2 within stem-like, tumor-initiating cells of glioma are regulated by phosphorylation of a triple serine motif in the Olig2 amino terminus at S10, S13, and S14. Phosphorylation of this motif is developmentally regulated and it is the phosphorylated form of Olig2 that has gliomagenic and anti-p53 functions (Sun et al., 2011). A more recent study demonstrates that this phosphorylation also regulates the switch from the proliferation to invasion in glioma cells (Singh et al., 2016). In studies summarized here, we use mass spectrometry (MS), genetics, and test-tube biochemistry with synthetic peptides to identify a set of three protein kinases that are collectively both necessary and sufficient to phosphorylate the triple serine motif. We go on to show that the motif, when phosphorylated, serves as a template to prime phosphorylation of three adjacent serines, thus creating a highly charged "acid blob" in the Olig2 amino terminus. Finally, we show that small molecule inhibitors of Olig2 protein kinases might have potential as glioma therapeutics.

## RESULTS

### Olig2 Is Phosphorylated by GSK3 at S10

We interrogated the Olig2 triple serine motif and flanking amino acids using four different computer algorithms to identify candidate protein kinases for S10, S13, and S14 (Table S1). Small molecule inhibitors of the most frequent hits in this in silico screen were tested on Olig2-positive neural progenitor cells (NPCs) (Table S2). Lysates of the drug-treated cells were size fractionated by SDS-PAGE and immunoblotted with a phospho-specific antibody that recognizes Olig2 only when all three members of the triple serine motif are in a phosphorylated state (Sun et al., 2011). These procedures identified S10 as a potential substrate for glycogen synthase kinase 3 (GSK3).

In mammals, two isoforms of GSK3 (α and β) share a high degree of homology, particularly in their kinase domain (Doble and Woodgett, 2003). As shown in Figures 1A and 1B, small molecule inhibitors of GSK3α/β and also lithium (a well-known GSK3α/β antagonist) suppress the phosphorylation of Olig2 in cultured mouse NPCs and also in low-passage human glioma cells (the BT145 line) that have been maintained under conditions developed for neural progenitors so as to maintain "stemness" (see the Experimental Procedures). *GSK3α*-null mice are viable (MacAulay et al., 2007), but *GSK3β*-null mice die at an early stage of embryonic development (Hoeflich et al., 2000). Accordingly, genetic validation of the GSK3 inhibitor data were achieved in NPC lines derived from informative intercrosses of GSKα-null and GSK3β-conditional mice, as shown schematically in Figure 1C. *GSK3α/β* double-knockout cells do not survive (Figure 1C), and immunoblotting assays show no change in phospho-Olig2 levels within GSK3α homozygous null NPCs (Figures 1D and 1E). However, we observe a significant reduction in phospho-Olig2 levels within $GSK3\alpha^{-/+}$; $GSK3\beta^{-/-}$ NPCs. Together, these findings indicate that GSK3 function is essential for phosphorylation of Olig2 and that GSK3α and β function redundantly toward this end.

To test whether Olig2 is directly phosphorylated by the GSK3s, we turned to in vitro kinase assays. As indicated in Figure 1F, the canonical substrates for GSK3α/β require a "priming" phosphoserine or phosphothreonine at +4 residues to the carboxyl side. In its phosphorylated state, S14 of Olig2 would serve this priming function. As shown in Figure 1G, recombinant GSK3β cannot phosphorylate an unmodified synthetic peptide corresponding to residues 1–18 of Olig2. However, an equivalent peptide with pre-phosphorylated S14 is an excellent substrate. Moreover, mass spectrometric analysis of the resulting products confirms that S10 is the enzymatic target of GSK3β in vitro. Besides singly phosphorylated S14, doubly phosphorylated peptides at S10 and S14 were detected when using phosphorylated S14 peptides as substrates (Figure 1H). Collectively, the data indicate that S10 of the Olig2 triple phosphoserine motif is phosphorylated by GSK3 and this requires pre-phosphorylation at S14.

### Olig2 Is Phosphorylated by Casein Kinase 2 at S13

Computer algorithms identified S13 as a potential substrate for casein kinase 2 (CK2) (Table S1). CK2 functions as a tetramer composed of two catalytic subunits, CK2α and CK2α′, and two copies of an essential regulatory subunit, CK2β (Litchfield, 2003). As indicated in Figures 2A and 2B, a small molecule inhibitor of CK2 (CX-4945) suppresses phosphorylation of Olig2 in murine NPCs and also in human glioma cells. Genetic validation of CK2 as an Olig2 kinase was achieved by using small hairpin RNA (shRNA) knockdown of CK2β, as shown in Figures 2C and 2D.

Canonical substrates for CK2 require priming by negatively charged amino acids such as aspartic acid (D), glutamic acid (E), or a phosphoserine (pS), positioned at either +1 or +3 residues to the carboxyl side (Figure 2E) (Meggio and Pinna, 2003). The primary sequence of Olig2 suggests that either E16 or phosphorylated S14 would prime S13 to be phosphorylated by CK2, and this prediction is borne out by in vitro kinase assays with recombinant CK2 showing that (1) S13 is a direct enzymatic target for CK2 and (2) CK2 phosphorylation of Olig2 at S13 is facilitated by pre-phosphorylation of S14 (Figures 2F and 2G). Of interest, mass spectrometric analysis of CK2-phosphorylated Olig2 peptides revealed that S3 is also a substrate for CK2, which is likely primed by aspartic acid at +1 residue to the carboxyl side.

### Cyclin-Dependent Kinases 1 and 2 Phosphorylate S14

As phosphorylation of the S10 and S13 sites was contingent upon prior phosphorylation of S14, we focused next on the identity of the S14 kinase. The S14 site precedes a proline residue, and phosphorylation of serine in this context is often mediated by so-called "proline-directed kinases." The known proline-directed kinases include mitogen-activated protein kinases (MAPKs) and cyclin-dependent kinases (CDKs). We focused on these particular kinase groups because phosphorylation of

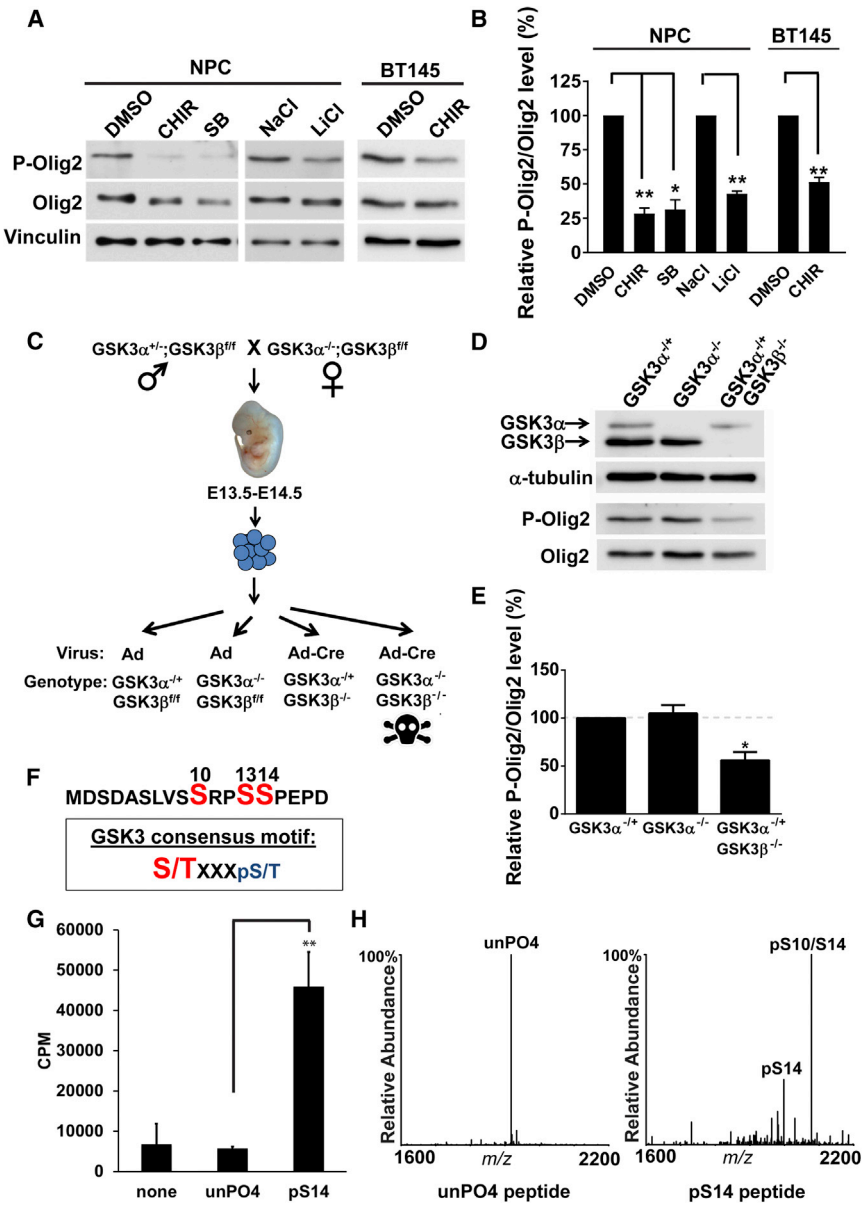


**Figure 1. GSK3 Phosphorylates Olig2 at S10**

(A) Immunoblot assay shows that inhibition of GSK3 results in reduced Olig2 phosphorylation. Mouse NPCs and BT145 human glioma cells treated with GSK3 inhibitors CHIR99021 (CHIR), SB216763(SB), or LiCl for 4 hr show a decrease in P-Olig2 level, compared to control cells that were treated with either DMSO or NaCl. The following concentrations were used: 5 μm CHIR, 10 μm SB, 10 mM NaCl, and 10 mM LiCl.

(B) Quantification of immunoblot assay. Relative P-Olig2/Olig2 levels were quantified and compared between control and inhibitor-treated groups. Data were analyzed by the Student's t test and are represented as the mean ± SEM. *$p < 0.05$; **$p < 0.01$ ($n = 3$). CHIR, CHIR99021; SB, SB216763.

(C) A schematic diagram shows generation of the mouse *GSK3α*- and *GSK3β*-knockout NPC lines. Control adeno (Ad) or adeno-Cre (Ad-Cre) virus was introduced to generate *GSK3α*- or *GSK3β*-knockout NPC lines.

(D) GSK3α and β function redundantly to phosphorylate Olig2. P-Olig2 levels were examined in $GSK3\alpha^{-/+}$, $GSK3\alpha^{-/-}$, and $GSK3\alpha^{-/+}GSK3\beta^{-/-}$ NPCs.

(E) Relative P-Olig2/Olig2 was quantified and compared between different groups. Data were analyzed by the Student's t test and are represented as the mean ± SEM. *$p < 0.05$ ($n = 3$).

(F) GSK3 consensus motif fits the S10 site upon phosphorylation at S14. pS, phosphorylated serine; S/T (highlighted in red), the kinase's target serine/threonine residue; X, any amino acid.

(G) In vitro kinase assay shows that GSK3 phosphorylates Olig2 N-terminal peptide; however, it requires a priming phosphorylation at S14. Synthetic Olig2 N-terminal peptides (aa 1–18) were used, and both unphosphorylated Olig2 N-terminal peptide (unPO4) and phosphorylated peptide at S14 (pS14) were tested. Reactions without peptides (none) served as negative control. Data were analyzed by the Student's t test and are represented as the mean ± SEM. **$p < 0.01$ ($n = 3$). aa, amino acid; counts per minute (CPM).

(H) Mapping the GSK3 phosphorylation sites by MS analysis. In vitro kinase reactions were analyzed by MALDI-MS and –MS/MS. The doubly phosphorylated peptide at S14 and S10 is indicated by pS14/S10. *m/z*, mass-to-charge ratio.

Olig2 is observed only in cycling or replication-competent cells (Sun et al., 2011).

As shown in Table S2, small molecule inhibitors of three major MAPKs, extracellular signal–regulated kinase 1/2 (ERK1/2), p38 MAPKs, and c-Jun N-terminal kinase (JNK) have no impact on the phosphorylation state of Olig2 in cycling NPCs. However, a subset of small molecule CDK antagonists suppresses Olig2 phosphorylation in murine NPCs and in the BT145 human glioma cell line. The active subset is confined to inhibitors that suppress the function of CDK1 and CDK2, whereas inhibitors active on other CDKs but not CDK1/2 show little or no activity on Olig2 phosphorylation (Figures 3A and 3B; Table S2). In these assays, phosphorylation of retinoblastoma protein (RB) served as a positive control for all CDK antagonists. Accordingly, CDK1 and CDK2 were singled out for genetic and biochemical validation.

For genetic validation, we first generated *CDK2*-null NPC lines from E13.5 embryos of *CDK2*-knockout mice (Berthet et al., 2003). As indicated in Figures S1A and S1B, loss of *CDK2* alone had no effect on Olig2 phosphorylation. Targeted disruption of *CDK1* leads to arrest of embryonic development at a very early stage (Santamaría et al., 2007). We tried chronic *CDK1* knockdown in NPCs by using shRNA targeting *CDK1*; however, the *CDK1*-knockdown cell lines also failed to thrive (data not shown). We then used an adeno-associated virus (AAV)-mediated shRNA for acute knockdown of *CDK1* in either wild-type or *CDK2*-null NPCs. As indicated in Figures 3C and 3D, acute shRNA knockdown of *CDK1* within *CDK2*-null NPCs significantly

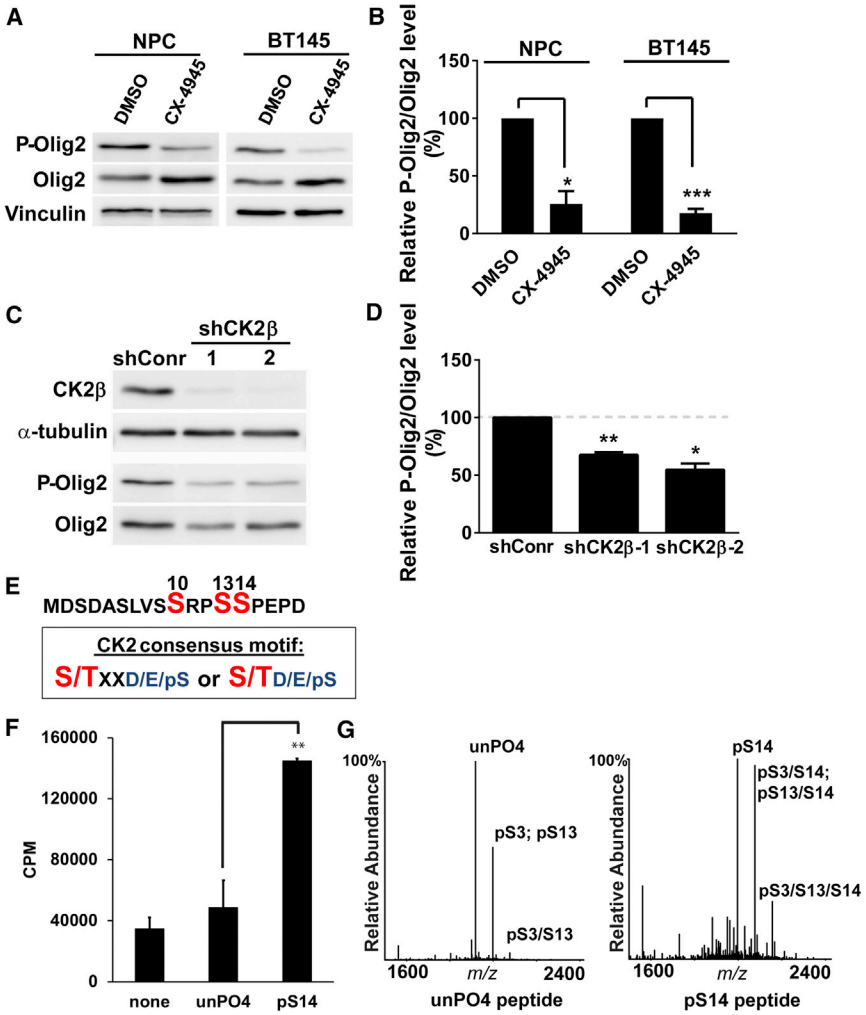


**Figure 2. CK2 Phosphorylates Olig2 at S13**

(A) Immunoblot assay. Mouse NPCs and BT145 human glioma cells were treated with the CK2 inhibitor CX-4945 (20 μM) for 4 hr. Cell lysates were size fractionated by PAGE and immunoblotted with P-Olig2 and Olig2 antibodies.

(B) Quantification of immunoblot assays. Relative P-Olig2/Olig2 levels were quantified and compared between control and inhibitor-treated group. Data were analyzed by the Student's t test and are represented as the mean ± SEM. *$p < 0.05$; ***$p < 0.001$ ($n = 3$).

(C) Genetic validation of inhibitor data. *CK2β* was knocked down in WT mouse NPCs by lentiviral vectors that express shRNAs targeting *mCK2β*. Cells that were stably transduced with lentivirus that encode non-target shRNA served as a control (shConr).

(D) Quantification of knockdown data. Relative P-Olig2/Olig2 levels were quantified and compared between the knockdown group and control group. Data were analyzed by the Student's t test and are represented as the mean ± SEM. *$p < 0.05$; **$p < 0.01$ ($n = 3$).

(E) CK2 consensus motif fits S13 site. D, aspartic acid; E, glutamic acid; pS, phosphorylated serine; S/T (highlighted in red), the kinase's target serine/threonine residue; X, could be any amino acid.

(F) In vitro kinase assay demonstrates that CK2 phosphorylates the Olig2 N-terminal peptide, and this phosphorylation is facilitated by the phosphorylation of S14. Synthetic Olig2 N-terminal peptides (aa 1–18) were generated without phosphorylation (unPO4) and with pre-phosphorylation at S14 (pS14). Reactions without peptides (none) served as negative control. Data were analyzed by the Student's t test and are represented as the mean ± SEM. **$p < 0.01$ ($n = 3$).

(G) Mapping CK2 phosphorylation sites by MS analysis. In vitro kinase reactions were analyzed by MALDI-MS and –MS/MS. Peaks shown are pS3 (singly phosphorylated peptide at S3), pS13 (singly phosphorylated peptide at S13), pS3/S13 (doubly phosphorylated peptide at S3 and S13), pS3/S14 (doubly phosphorylated peptide at S3 and S14), pS13/S14 (doubly phosphorylated peptide at S13 and S14), and pS3/S13/S14 (triply phosphorylated peptide at S3, S13 and S14).

reduced Olig2 phosphorylation, while acute knockdown of *CDK1* alone in wild-type cells had no effect on Olig2 phosphorylation (Figures S1C and S1D). Together, these results indicate that CDK1 and CDK2 function redundantly for phosphorylation of Olig2.

Despite repeated efforts, we were unable to establish assay conditions wherein recombinant CDK1 or CDK2 would function on synthetic peptides in vitro, which might be due to the short length of the Olig2 N-terminal peptide used in the assay. Accordingly, we used an in vivo phosphorylation assay with an analog-sensitive mutant of CDK2 (analogue-sensitive [AS]-CDK2) to validate Olig2 as a direct substrate for CDK2. The ATP-binding pocket of this mutant CDK2 can utilize bulky adenine analogs, such as ATP-γ-S as a phosphate donor, and can therefore label CDK2 substrate with P-γ-S (Merrick et al., 2011). Expression vectors encoding wild-type CDK2 or this analog-sensitive CDK2, together with V5-epitope-tagged wild-type Olig2 or the S14G Olig2 mutant, were transfected into 293 cells that do not express endogenous Olig2. Incorporation of P-γ-S into wild-type or mutant Olig2 was assessed by anti-thiophosphate ester antibody. As shown in Figures 3E and 3F, the analog-sensitive mutant CDK2 can phosphorylate wild-type Olig2, whereas the phosphorylation level is reduced upon mutation of the S14 site. These data indicate that S14 is a direct substrate for CDK2.

## Phosphorylation of the Triple Serine Motif Enables Formation of a Hexa-phosphoserine Acid Blob in the Amino Terminus of Olig2

During the course of this work, our procedures and protocols for mass spectrometric analysis of Olig2 were refined. Improved methodology enabled the detection of additional phosphoserine residues in the amino terminal end of Olig2 at S3, S6, and S9 (Figures 4A and S2). However, as shown in Figure 4A in NPCs expressing wild-type (WT) Olig2, peptide fragments with these additional phosphoserine residues were never observed without phosphorylations within the original S10, S13, and S14 sites.

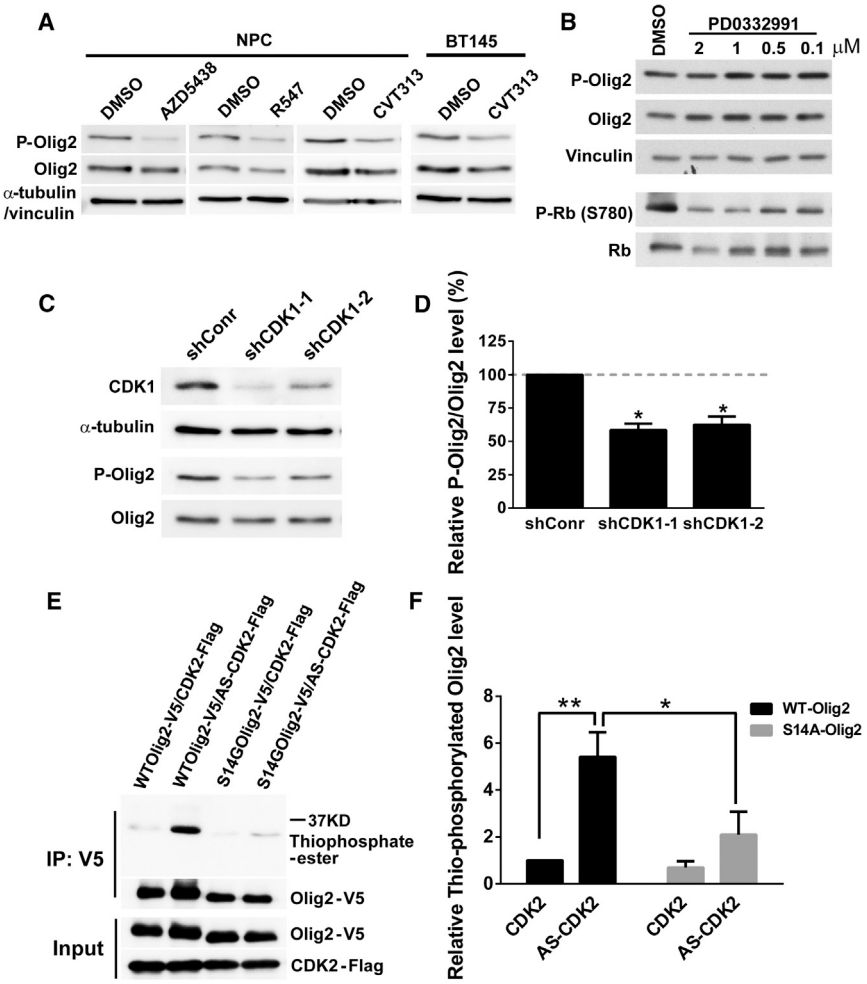


**Figure 3. S14 of Olig2 Is Phosphorylated by CDK1/2**

(A) Mouse NPCs and BT145 human glioma cells treated with CDK1/2 inhibitors show a decrease in P-Olig2 level: AZD5438 (CDK1/2/9 inhibitor), R547 (CDK1/2/4 inhibitor), CVT313 (CDK1/2 inhibitor). P-Olig2 and Olig2 levels were examined 4 hr after AZD5438 and R547 treatment or 24 hr after CVT313 treatment in NPCs and 3 hr after CVT313 treatment in BT145 cells. The following concentrations were used: 10 μm AZD5438, 5 μm R547, and 10 μM CVT313.

(B) Mouse NPCs treated with CDK4/6 inhibitor, PD0332991, show no obvious change in P-Olig2 level. P-Olig2 and Olig2 levels were examined 4 hr after PD0332991 treatment.

(C) Genetic validation of CDK1/2 inhibitor data. The immunoblot assay shows that knockdown of *CDK1* in *CDK2*-knockout NPCs decreases the P-Olig2 level. *CDK1* was acutely knocked down in *CDK2*-knockout NPCs by introducing AAV that expresses shRNA targeting *mCDK1*. Cells transduced with AAV that expresses non-target shRNA served as a control (shConr). P-Olig2 and Olig2 levels were examined at 48 hr after viral transduction.

(D) Quantification of knockdown data. Relative P-Olig2/Olig2 levels were quantified and compared between the knockdown group and control group. Data were analyzed by the Student's t test and are represented as the mean ± SEM. *$p < 0.05$ ($n = 3$).

(E) An analog-sensitive kinase assay shows that CDK2 phosphorylates Olig2 at the S14 site.

(F) Quantification of analog-sensitive kinase assays. Thiophosphorylated Olig2 levels were quantified, normalized to total Olig2, and then compared between different groups. Data were analyzed by two-way ANOVA with the Sidak post test and are represented as the mean ± SEM. *$p < 0.05$; **$p < 0.01$ ($n = 4$).

The relationship of S3, S6, and S9 to the phosphorylation state of the original triple serine motif was assessed in a set of "contingency" assays. Olig2-null NPCs were transduced with lentiviral expression vectors encoding Olig2 mutants with informative phospho-null substitutions at S10, S13, or S14. As shown in Figure 4A, ablation of the original triple serine motif completely eliminates phosphorylation at S3, S6, and S9. Phospho-null substitutions at S13 and S14 ablate the phosphorylation of S10 and likewise ablate phosphorylation of S6 and S9. Finally, a single S→G substitution at S14 almost completely eliminates phosphorylation at S10 and S13, although there is a low level of "breakthrough" phosphorylation events to the amino terminal side. This is consistent with the CK2 kinase assay, which suggests that S13 and S3 can be phosphorylated even with the absence of S14 phosphorylation, although the efficiency is relatively low (Figures 2F and 2G).

The contingency relationships of S10 and S13 to the phosphorylation state of S14 are predicted by the priming requirements of GSK3 and CK2 (see Figures 1 and 2). Moreover, close scrutiny of the Olig2 amino acid sequence shows that S10 and S13, when phosphorylated, could themselves serve to prime S6 and S9 for phosphorylation by GSK3 and CK2. In addition, phosphorylation of S6 would facilitate CK2 phosphorylation on S3. Thus, as modeled in Figure 4B, phosphorylation of S14 by the cell cycle-modulated kinase CDK1/2 initiates formation of a hexa-phosphate acidic domain in the amino terminus of Olig2.

## Therapeutic Potential for Small Molecule Inhibitors of Olig2 Phosphorylation

The phosphorylation state of Olig2 is developmentally regulated, being high in cycling neural progenitors and low in terminally differentiated, myelinating oligodendrocytes. Previous studies have shown that gliomagenic and anti-p53 functions of Olig2 are contingent upon phosphorylation of the triple serine motif (Sun et al., 2011). The functional relevance of this relationship to the pathobiology of human glioma is illustrated by an oppositional relationship between phospho-Olig2 and p53 status. As shown in Figure 5, the phospho-Olig2 content of gliomas with genetically intact p53 is more comparable to that of cycling neural progenitors than to myelinating oligodendrocytes and is significantly higher than that of p53 mutant gliomas.

Are therapeutic opportunities for glioblastoma embedded in the kinases that phosphorylate the triple serine motif? To address this question, we turned to the genetically accessible

A

| Phospho-Residues | WT | TPN | DPN | SPN |
|---|---|---|---|---|
| pS10 | + | - | - | +/- (≤10%) |
| pS13 | + | - | - | +/- (≤10%) |
| pS14 | + | - | - | - |
| pS10/S14 | + | - | - | - |
| pS13/S14 | + | - | - | - |
| pS10/S13 | + | - | - | - |
| pS10/S13/S14 | + | - | - | - |
| pS9/S10/S13 | + | - | - | - |
| pS9/S10/S14 | + | - | - | - |
| pS3/S10/S14 | + | - | - | - |
| pS9/S10/S13/S14 | + | - | - | - |
| pS6/S10/S13/S14 | + | - | - | - |
| pS3/S6/S10/S14 | + | - | - | - |
| pS3/S10/S13/S14 | + | - | - | - |
| pS6/S9/S10/S13/S14 | + | - | - | - |
| pS3/S6/S9/S10/S13/S14 | + | - | - | - |
| pS3 | - | - | + | + |
| pS6 | - | - | - | - |
| pS9 | - | - | - | - |
| pS3/S6 | - | - | - | + |
| pS3/S9 | - | - | - | - |
| pS6/S9 | - | - | - | - |
| pS3/S6/S9 | - | - | - | - |

B

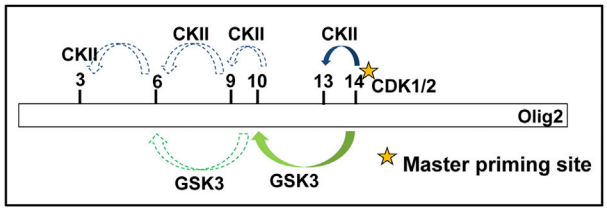


**Figure 4. Phosphorylation of the Triple Serine Motif Enables Formation of a Hexa-phosphoserine Acid Blob in the Amino Terminus of Olig2**

(A) Summary of mass spectrometric analyses on Olig2 N-terminal phosphorylated peptides detected in *Olig2*-null NPCs that were transduced with WT, triple phospho null (TPN) (S10A/S13A/S14G), double phospho null (DPN) (S13A/S14G), or single phospho null (SPN) (S14G) Olig2. Black font, phosphorylated peptides identified in previous study (Sun et al., 2011); red font, newly identified phosphorylated peptides in WT-Olig2 sample; blue font, contingent phospho peptides that are undetectable or barely detectable in WT-Olig2 sample. +, present; +/−, detected but with low level; −, undetectable.

(B) A sequentially priming phosphorylation cascade. A schematic diagram shows how the triple serine motif creates priming sites for additional phosphorylations at S3, S6, and S9 that create a hexaphosphate acid blob in the Olig2 amino terminus.

murine NSCs. The anti-p53 functions of Olig2 manifest themselves in short-term assays and are quantifiable by suppression of p21 expression. As shown in Figure 6, small molecule inhibitors of CDK1/2, CK2, and GSK3$\alpha$/$\beta$ all trigger elevated expression of p21. Although these small molecule inhibitors likely suppress the phosphorylation of multiple on-target and off-target protein substrates, the p21 responses shown in Figure 6 are largely rescued by expression of a triple phosphomimetic

A

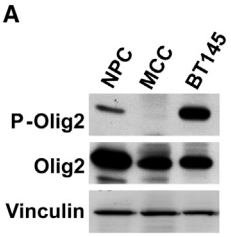


B

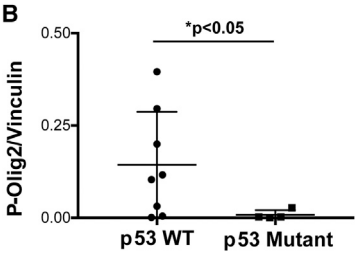


**Figure 5. Analysis P-Olig2 Levels in a Panel of Glioma Cells with Either WT p53 or Mutant p53**

(A) Immunoblot of P-Olig2 in cycling neural progenitor cells (NPCs), adult mouse corpus callosum (MCC), and low-passage human glioma cells (BT145 line).

(B) Glioma cell lines with intact p53 have significantly higher level of P-Olig2 than p53 mutant glioma cells. The relative P-Olig2/Vinculin levels were analyzed and compared in different glioma cell lines. Data were analyzed by the Mann-Whitney test and are represented as the mean ± SEM. *p < 0.05 (n = 8 p53 WT glioma cell lines [filled circles] and n = 4 p53 mutant cell lines [filled boxes]).

(TPM) Olig2 (S10D/S13E/S14D), indicating that the drug effects on p21 expression are channeled, at least in part, through their action on Olig2.

To assess effects of the kinase inhibitors on cell proliferation, we used a preclinical murine model of pediatric glioma, a common Olig2-positive brain tumor of childhood (Bergthold et al., 2014). Activating mutations within the BRAF serine/threonine protein kinase (BRAFV600E) and homozygous deletion of Ink4a/ARF co-occur in a subset of World Health Organization (WHO) grade II–IV pediatric diffuse astrocytomas (Schiffman et al., 2010). Mouse NPCs bearing these two mutations are tumorigenic, and the resulting tumors recapture the histological characteristics and cellular markers (e.g., Olig2, glial fibrillary acidic protein (GFAP), and Nestin) of human pediatric glioma (Huillard et al., 2012). We therefore utilized this mouse model to assess therapeutic potential of the triple serine motif as a drug target. Of the six small molecule kinase inhibitors studied here, the CK2 inhibitor CX-4945 scored second highest on the CNS multiparameter optimization (MPO) algorithm for brain penetrance (Wager et al., 2010) (Table S3). Moreover, CX-4945 is the only one among the six small molecule kinase inhibitors currently in clinical trials (Chon et al., 2015). Accordingly, our studies with this tumor model focused on CX-4945.

To address brain penetrance of CX-4945, we first monitored Olig2 phosphorylation in the brains of drug-treated mice. As shown in Figures 7A and 7B, CX-4945 treatment significantly reduces P-Olig2-positive cells in the brain of our glioma mouse model. Next, we sought to determine whether CX-4945 could inhibit cell proliferation in our tumor model by regulating P-Olig2 levels. This was addressed by using two knockin lines, wherein the coding sequence of either WT Olig2 or TPM Olig2 (S10D/S13E/S14D, TPM-Olig2) was introduced into the Olig2 locus. As shown in Figures 7C and 7D, CX-4945 inhibits tumor cell proliferation, but the growth inhibition is rescued by the TPM-Olig2 variant. As noted for the studies on p21 expression (Figure 6), the TPM-Olig2 rescue of proliferation is only partial,

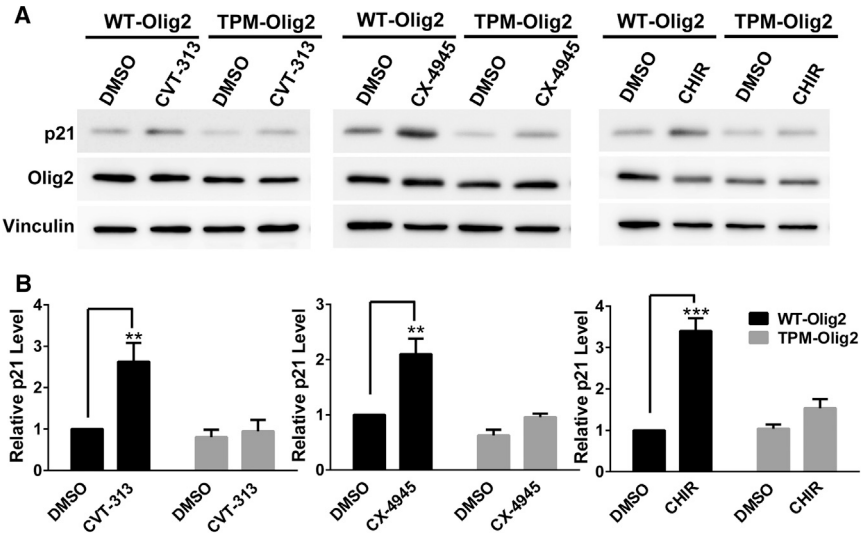


**Figure 6. Inhibition of Olig2 Phosphorylation Enhances p53 Function**

(A) Olig2 kinase inhibitors increase the p21 level through inhibiting Olig2 phosphorylation. *Olig2*-null NPCs were transduced with retroviruses that express either WT-Olig2 or TPM-Olig2. The activation state of p21 upon kinase inhibitor treatment was examined and compared between two NPC lines by western blot analysis. Cells were examined either after 24-hr treatment with 5 μM CVT313 (CDK1/2 inhibitor) or after 8-hr treatment with 10 μM CX-4945 (CK2 inhibitor) or 5 μM CHIR99021 (GSK3 inhibitor).

(B) Quantification of immunoblot assay. Data were analyzed by two-way ANOVA with the Sidak post test. There is a significant difference between WT-Olig2 and TPM-Olig2 in response to Olig2 kinase inhibitors. Data are represented as the mean ± SEM. $^{**}p < 0.01$; $^{***}p < 0.001$ (n = 3).

presumably because the impact of a CK2 antagonist such as CX-4945 is not confined to Olig2.

With respect to tumor growth in vivo, previous studies have shown that PLX-4720 (a small molecule RAF inhibitor that is currently in clinical trials for BRAF mutant pediatric astrocytoma; Penman et al., 2015) prolongs survival of mice that received intracranial grafts of the tumor cells (Bergthold et al., 2014). As shown in Figures 7E and 7F, CX-4945, as a single agent, had no statistically significant impact on survival of mice that were challenged with the tumor cells. However, CX-4945 cooperated with PLX-4720 to give a survival benefit that exceeds that delivered by the RAF inhibitor alone. Collectively, these data suggest therapeutic potential for drugs that block phosphorylation of the triple serine motif, either as adjuvants to radiation and chemotherapy or in combination with other targeted therapeutics.

## DISCUSSION

During development and also in disease, pro-mitogenic/anti-p53 functions of Olig2 are controlled by phosphorylation of a triple serine motif at the amino terminus of the protein (Mehta et al., 2011; Sun et al., 2011). Here we identify a set of three protein kinases that are both necessary and sufficient to phosphorylate the triple serine motif. We go on to show that in its phosphorylated state, the triple serine motif serves as a template that enables phosphorylation of an additional three serines including S9, S6, and S3, generating a hexa-phosphoserine acidic domain in the Olig2 amino terminus. A broad body of data document the functional role of acidic domains (a.k.a. "acid blobs" or "negative noodles") as facilitators of protein-protein interactions that enable transcription factor function (Banerjee and Kundu, 2003; Cross et al., 2011; García-Rodríguez and Rao, 1998; Li and Botchan, 1993; Sigler, 1988). Protein alignment of Olig2 shows complete conservation of the six serines in the amino terminal acid blob among humans, mice, chickens, frogs, and fish (Meijer et al., 2012). Formation of the Olig2 acid blob is linked to the cell cycle by CDK1/2-mediated phosphorylation of S14.

The three kinases that phosphorylate the triple serine motif are broadly expressed, and direct evidence of their developmental functions in the formation of Olig2-dependent cell types is lacking. However, targeted disruption of the CK2 regulatory subunit CK2β in embryonic stem cells does recapitulate some features of the Olig2-null mouse, including compromised NPC proliferation and oligodendrogenesis (Huillard et al., 2010).

On a more practical note, a broad body of data suggest that Olig2 would be an attractive target for glioma therapeutics (Ligon et al., 2007; Mehta et al., 2011; Suvà et al., 2014). *Olig2*-null mouse embryos develop to term but die within minutes following birth, due to a total deficit of motor neurons (Lu et al., 2002; Zhou and Anderson, 2002). However, ablation of Olig2 in the postnatal mouse brain is survivable for extended periods of time (Cai et al., 2007). Moreover, as a glioma therapeutic, an Olig2 antagonist might be required only transiently as an adjuvant to standard-of-care therapeutics. Transcription factors per se are difficult targets for drug development because their interactions with DNA or co-regulator proteins tend to involve large surface areas. However, protein kinases lend themselves well to development of targeted therapeutics. Does the Olig2 acid blob constitute a therapeutic opportunity for glioma?

Data generated with small molecule inhibitors of the triple serine motif kinases can be correlated with a mutational analysis conducted by Sun et al. (2011). Using site-directed mutagenesis, Sun et al. (2011) found that a triple phospho-null mutation (S10G/S13A/S14A) had a severe proliferation phenotype and a double phospho-null mutation (S13A/S14G) had a partial proliferation phenotype, whereas a single phospho-null substitution at S14 (S14G) had no discernable impact on cell proliferation. The lack of a phenotype with the S14G mutation is somewhat at odds with the pivotal role of S14 as "the first domino" to fall in a sequentially priming, forward-feeding phosphorylation cascade as shown in Figure 4. However, the negative result may be explained by the MS data summarized in Figure 4A, which suggest a low level of "breakthrough" phosphorylation events to the amino terminal side of the S14G substitution. The

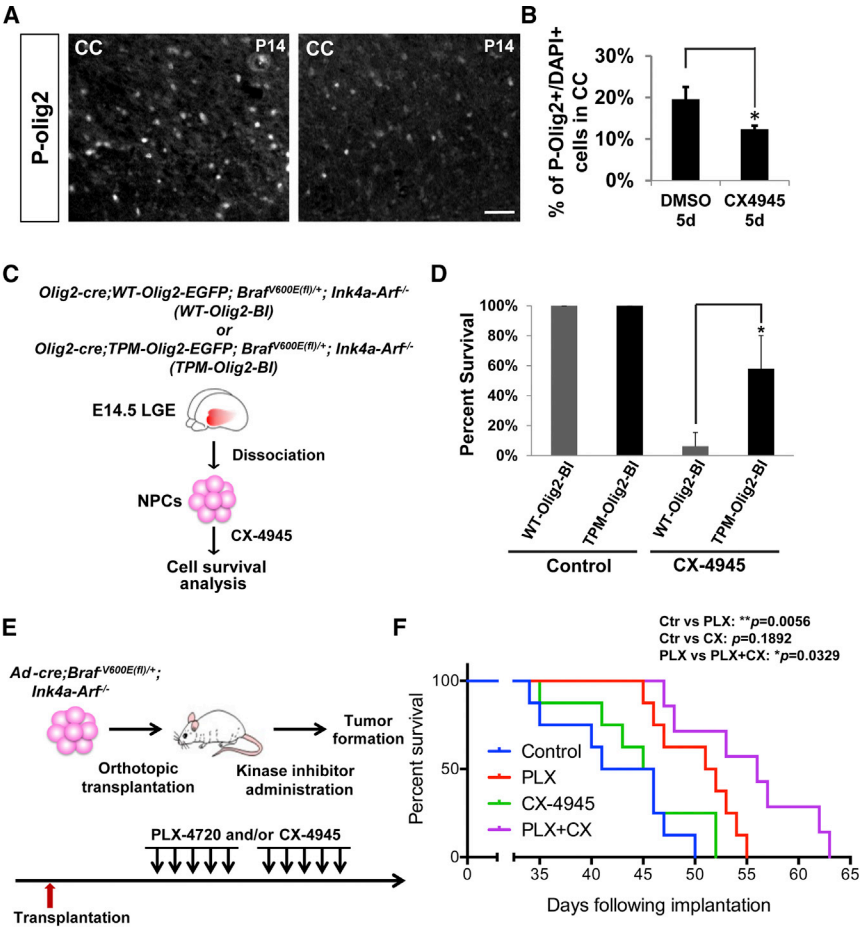


**Figure 7. Therapeutic Potential of an Olig2 Kinase Antagonist in a Murine Model of Pediatric Low-Grade Astrocytoma**

(A) CK2 inhibition decreases the P-Olig2 level in vivo. Developing *hGFAP-cre; BrafV600E$^{(fl)/+}$; Ink4a-Arf$^{-/-}$* pups were treated with 25 mg/kg of CK2 inhibitor CX-4945 intraperitoneally for 5 days and were analyzed at P14.

(B) Quantification of P-Olig2 immunostaining. Data are represented as the mean ± SD. *p < 0.05 (n = 3). CC, corpus callosum. Scale bar, 50 μm.

(C) A schematic diagram shows generation of two *BRAFV600E*-transformed NPC lines in an *Ink4a-Arf$^{-/-}$* background. The two lines express knockin, epitope-tagged Olig2, wherein the triple serine motif is either WT (WT-Olig2-BI) or TPM with the S10D/S13E/S14D substitutions (TPM-Olig2-BI). Of note, the *Olig2-cre* driver is used to activate expression of the BRAFV600E oncogene, while simultaneously disrupting another endogenous Olig2 allele (Schüller et al., 2008). The resulting mice exhibit early prenatal lethality, which precludes further study in postnatal pups.

(D) Proliferation of the TPM-Olig2-BI line is partially resistant to the CK2 antagonist CX-4945. For proliferation assays, 5 × $10^4$ cells were seeded at day 0 and 1 μM CX-4945 was added at day 1. The cell number was assessed at day 4. Data were analyzed by the Student's t test and are represented as the mean ± SD. *p < 0.05 (n = 3).

(E) A schematic diagram demonstrates orthotopic transplantation and the treatment regimen (see the Experimental Procedures).

(F) Combination of BRAF and CK2 inhibitors significantly improves survival in an orthotopic model of pediatric glioma. A Kaplan-Meier graph is illustrated and the log-rank test was used to determine the survival differences between different treatment groups. *p < 0.05; **p < 0.01 (n = 8).

partial loss of proliferative ability exhibited by the double phospho-null substitution at S13/S14 (Sun et al., 2011) is in accord with the Figure 4A data, showing that double substitution delivers a more complete suppression of phosphorylation events at S3, S6, S9, and S10. It should also be noted that the cells may adapt to chronic (i.e., genetic) loss of P-Olig2 in ways that cannot be achieved with acute, drug-induced loss.

Against this genetic backdrop, small molecule inhibitors targeted to any one of the three kinases that are essential to formation of the acid blob stimulate expression of p21 (a canonical p53 target gene) and this effect is channeled, at least in part, through phosphorylation of the Olig2 triple serine motif (Figure 6). Among these kinase inhibitors, the selective CK2 inhibitor, CX-4945, is orally available and has been on clinical trials for multiple solid tumors. Although it has not been tested clinically in glioma, CK2α is frequently overexpressed in glioblastoma, particularly in the classical subtype of glioma (50.7%) (Zheng et al., 2013). In preclinical studies, CK2 demonstrates an important role in regulating glioma cell viability and is necessary for glioma tumorigenesis in vivo. Inhibition of CK2 by CX-4945 impairs glioma cell proliferation in vitro and suppresses human glioma growth in the xenograph model (Dixit et al., 2012; Nitta et al., 2015; Zheng et al., 2013). In our study, we further tested CX-4945 in a pediatric astrocytoma model. As shown in Figure 7, CX-4945 inhibits proliferation of Olig2-positive tumor cells and cooperates with a targeted BRAF antagonist to improve survival in a murine model of BRAF mutant pediatric astrocytoma. Collectively, the genetic and pharmacologic data suggest that small molecule inhibitors of the triple serine motif protein kinases could have therapeutic potential for malignant gliomas, either as standalone modalities or as adjuvants to radiotherapy, genotoxic drugs, and targeted therapeutics.

## EXPERIMENTAL PROCEDURES

### Kinase Inhibitors

The serine kinase inhibitors used in this study were AZD5438 (CDK1/2/9 inhibitor; Selleckchem), R547 (CDK1/2/4 inhibitor; Selleckchem), CVT313 (CDK1/2 inhibitor; EMD Millipore), PD0332991 (CDK4/6 inhibitor; Selleckchem), CX-4945 (CK2 inhibitor; Selleckchem or Pfizer), CHIR99021 (GSK3 inhibitor; Selleckchem), SB216763 (GSK3 inhibitor; Selleckchem), PLX-4720 (BRAFV600E inhibitor; Plexxikon), and LiCl (GSK3 inhibitor; Sigma). All of the small molecule inhibitors were dissolved in DMSO and stock solutions were kept at −20°C, except LiCl, which was dissolved in water and kept at room temperature.

### NPC and Human Glioma Cell Culture

Mouse NPCs were isolated from the lateral ganglionic eminence (LGE) of E13.5–E14.5 embryos. All human glioma cell lines were provided by Dr. Ligon's

group (Brigham and Women's Hospital) and were originally derived from Brigham and Woman's Hospital patients undergoing surgery in accordance with institutional review board (IRB) protocols. Both NPCs and human glioma cells were cultured in serum-free medium containing B27 and N2 supplements, epidermal growth factor (EGF; 20 ng/mL), and basic fibroblast growth factor (bFGF; 20 ng/mL). Cells were grown on laminin-coated plates to maintain an adherent monolayer culture for most assays, except for the experiments shown in Figure 5, where glioma cells were grown as neurosphere cultures.

### Animals

All animal handling and procedures were performed according to University of North Carolina (UNC), Dana-Farber Cancer Institute (DFCI), Northwestern University (NWU) Feinberg School of Medicine, or University of California, San Francisco (UCSF) guidelines under Institutional Animal Care and Use Committee (IACUC)-approved protocols.

### *GSK3*-Null NPC Lines

To generate *GSK3*$\alpha/\beta$-null NPC lines, we crossed *GSK3*$\alpha^{+/-}$; *GSK3*$\beta^{floxP/floxP}$ male and *GSK3*$\alpha^{-/-}$; *GSK3*$\beta^{floxP/floxP}$ female mice (Kim et al., 2009; MacAulay et al., 2007; Patel et al., 2008) and derived *GSK3*$\alpha^{+/-}$; *GSK3*$\beta^{floxP/floxP}$ or *GSK3*$\alpha^{-/-}$; *GSK3*$\beta^{floxP/floxP}$ NPCs from the LGE of individual E13–E14 embryos. To generate *GSK3*$\beta$-null NPC lines, we infected the above cell lines with either adenovirus that expresses the *Cre* recombinase gene or adenovirus only. The ratio of virus to cells was 100:1. Transduced cells were cultured for at least three passages before examination to ensure complete recombination for the *GSK3*$\beta$ locus.

### In Vitro Peptide Kinase Assay

Active kinases, GSK3β and CK2, were purchased from either Promega (GSK3β, V1991) or New England Biolabs (CK2, P6010L). Peptides that cover 18 amino acids of the N terminus of Olig2 protein were synthesized as either native peptides or phosphorylated peptides at S14 (Tufts Physiology Core). For kinase reactions, we mixed active kinase, Olig2 N-terminal peptides (20 mM) and $^{32}$P-labeled ATP (3,000 Ci/mmol) in reaction buffer, and then incubated the mixture for 15 min at 30°C. Reactions were then blotted onto nitrocellulose membrane and washed three times with 150 mM phosphoric acid, dried, and subjected to liquid scintillation counting. The products of cold peptide kinase assays were subjected to MALDI-MS and tandem mass spectrometry (–MS/MS) analyses to identify the phosphorylation site(s) (see the Supplemental Experimental Procedures).

### Analog-Sensitive Kinase Assay with CDK2

WT-CDK2 and AS-CDK2 (F80G) were expressed by the p3xFLAG-CMV (Sigma) vectors. WTOlig2-V5 and S14GOlig2-V5 were cloned into pcDNA backbone vectors. To test whether CDK2 can phosphorylate Olig2, we transfected 293 cells with WTOlig2-V5 or S14GOlig2-V5 with either WT-CDK2-Flag or AS-CDK2-Flag. The in vivo phosphorylation assay was performed according to a previous protocol with slight modification (Banko et al., 2011) (see the Supplemental Experimental Procedures).

### Olig2 Protein Purification

As described previously, we have cloned full-length and different mutant forms of Olig2 into the pWZL-blast retrovirus vector (Sun et al., 2011). We generated mouse NPC lines that stably express either WT or different mutant forms of Olig2 by transducing Olig2-null NPCs with the appropriate virus. Exogenous Olig2 proteins contain a V5 tag at the C terminus. For MS analysis, we isolated the nuclear fraction and purified Olig2 by using anti-V5 agarose affinity gel (Sigma). The immunoprecipitation (IP) samples were then digested and subjected to nano-liquid chromatography (LC)-electrospray ionization (ESI)-MS analysis for phospho-Olig2 peptides.

### Preclinical Murine Models of Pediatric Low-Grade Astrocytoma

*BRAFV600E* in the context of *Ink4a-Arf*$^{-/-}$ is a common genetic driver set for pediatric glioma (Huillard et al., 2012). *Braf*$^{V600E(fl)/+}$ mice, *Ink4a-Arf*$^{-/-}$ mice, and *Olig2-cre* mice have been described previously (Dankort et al., 2007; Schüller et al., 2008; Serrano et al., 1996). Two knockin mouse lines that express either WT-Olig2 or TPM-Olig2 (S10D/S13E/S14D) fused to internal ribosome entry site (IRES)-EGFP cassettes were newly generated through homologous recombination of the Olig2 locus in embryonic stem cells (ESCs). Of note, Olig2-cre; *Braf*$^{V600E(fl)/+}$; *Ink4a-Arf*$^{-/-}$ mice exhibit early prenatal lethality. However, by intercrossing the above mouse lines (see the schematic in Figure 7C), we were able to generate *Olig2-cre;WT-Olig2-EGFP;Braf*$^{V600E(fl)/+}$; *Ink4a-Arf*$^{-/-}$ and *Olig2-cre;TPM-Olig2-EGFP;Braf*$^{V600E(fl)/+}$; *Ink4a-Arf*$^{-/-}$ embryos and isolate NPCs from E14.5 LGE. These Olig2 knockin cell lines (labeled WT-Olig2-BI or TPM-Olig2-BI) were used for in vitro proliferation assays.

For in vivo drug tests, we used adenovirus-Cre to activate *BRAFV600E* within NPCs isolated from *Braf*$^{V600E(fl)/+}$;*Ink4a-Arf*$^{-/-}$ embryos (see the schematic in Figure 7E). 2 × 10$^5$ cells were injected into the brains of 6-week-old immunodeficient (nude) mice as previously described (Hashizume et al., 2010). Mice were randomly assigned to four cohorts and treated with 20 mg/kg PLX-4720 and/or 25 mg/kg CX-4945 by intraperitoneal injection for 5 consecutive days (Monday to Friday) for 2 weeks starting 5 days after transplantation. All mice were monitored daily for the development of symptoms related to tumor growth. Mice were euthanized when they exhibited symptoms indicative of significant impairment in neurological function.

### Statistical Methods

Differential levels of P-Olig2 levels in glioma cell lines were analyzed by the Mann-Whitney test. Two-way ANOVA with Sidak post tests was performed when analyzing the analog-sensitive kinase assays and when comparing the response of WT-Olig2 and TPM-Olig2 cell lines to Olig2 kinase inhibitors. The log-rank test was used to determine the survival differences between different treatment groups of mice, and Student's t tests were used to analyze sample differences in other assays as described in the figure legends. The statistical values were obtained using GraphPad Prism software.

## SUPPLEMENTAL INFORMATION

Supplemental Information includes Supplemental Experimental Procedures, two figures, and three tables and can be found with this article online at http://dx.doi.org/10.1016/j.celrep.2017.03.003.

## AUTHOR CONTRIBUTIONS

J.Z. identified the kinases involved in phosphorylating Olig2; A.-C.T. tested Olig2 kinases in vivo in pediatric glioma model cells; J.A.A. did the in vitro kinase assays; S.B.F., J.D.C., and J.A.M. performed the MS experiments; A.G. set up the mouse tumor system; J.S.D. provided technical assistance; M.M.-S. and W.D.S. provided GSK3 knockout embryos; W.M. and P.S. provided the analog-specific kinase system and helpful discussions; K.L.L. offered the human glioma cell lines; Y.S. and J.A.A. examined and analyzed the P-Olig2 levels in different p53 WT and p53 mutant glioma cell lines; R.H. and C.D.J. performed the orthotopic survival study; and J.Z., D.H.R., and C.D.S. designed the experiments and wrote the paper.

## ACKNOWLEDGMENTS

The authors thank Philipp Kaldis for the *CDK2*-knockout mice and Martin McMahon for *Braf*$^{V600E(fl)/+}$ mice. Nathanael Gray, Sara Buhrlage, Tinghu Zhang, Jinhua Wang, and Per Hydbring contributed useful suggestions on kinase inhibitors. Expert technical assistance and advice was provided by Krister Barkovich, Sandra Chang, and Emmanuelle Huillard. We thank the American Brain Tumor Association for postdoctoral fellowship support (to A.-C.T.) and the American Association for Cancer Research (AACR) for a Anna D. Baker Fellowship in Basic Cancer Research (to A.G.). This work was supported by grants from NIH (NS057727 to C.D.S. and NS040511 to D.H.R.) and by funding from the Dana-Farber Strategic Research Initiative (to J.A.M.), Howard Hughes Medical Institute (to D.H.R.), and A Kids' Brain Tumor Cure Foundation (to C.D.S.).

Received: July 22, 2016
Revised: November 14, 2016
Accepted: February 28, 2017
Published: March 28, 2017

## REFERENCES

Banerjee, S., and Kundu, T.K. (2003). The acidic C-terminal domain and A-box of HMGB-1 regulates p53-mediated transcription. Nucleic Acids Res. *31*, 3236–3247.

Banko, M.R., Allen, J.J., Schaffer, B.E., Wilker, E.W., Tsou, P., White, J.L., Villén, J., Wang, B., Kim, S.R., Sakamoto, K., et al. (2011). Chemical genetic screen for AMPKα2 substrates uncovers a network of proteins involved in mitosis. Mol. Cell *44*, 878–892.

Bergthold, G., Bandopadhayay, P., Bi, W.L., Ramkissoon, L., Stiles, C., Segal, R.A., Beroukhim, R., Ligon, K.L., Grill, J., and Kieran, M.W. (2014). Pediatric low-grade gliomas: how modern biology reshapes the clinical field. Biochim. Biophys. Acta *1845*, 294–307.

Berthet, C., Aleem, E., Coppola, V., Tessarollo, L., and Kaldis, P. (2003). Cdk2 knockout mice are viable. Curr. Biol. *13*, 1775–1785.

Bouvier, C., Bartoli, C., Aguirre-Cruz, L., Virard, I., Colin, C., Fernandez, C., Gouvernet, J., and Figarella-Branger, D. (2003). Shared oligodendrocyte lineage gene expression in gliomas and oligodendrocyte progenitor cells. J. Neurosurg. *99*, 344–350.

Cai, J., Chen, Y., Cai, W.H., Hurlock, E.C., Wu, H., Kernie, S.G., Parada, L.F., and Lu, Q.R. (2007). A crucial role for Olig2 in white matter astrocyte development. Development *134*, 1887–1899.

Cancer Genome Atlas Research Network (2008). Comprehensive genomic characterization defines human glioblastoma genes and core pathways. Nature *455*, 1061–1068.

Chon, H.J., Bae, K.J., Lee, Y., and Kim, J. (2015). The casein kinase 2 inhibitor, CX-4945, as an anti-cancer drug in treatment of human hematological malignancies. Front. Pharmacol. *6*, 70.

Cross, B., Chen, L., Cheng, Q., Li, B., Yuan, Z.M., and Chen, J. (2011). Inhibition of p53 DNA binding function by the MDM2 protein acidic domain. J. Biol. Chem. *286*, 16018–16029.

Dankort, D., Filenova, E., Collado, M., Serrano, M., Jones, K., and McMahon, M. (2007). A new mouse model to explore the initiation, progression, and therapy of BRAFV600E-induced lung tumors. Genes Dev. *21*, 379–384.

Dixit, D., Sharma, V., Ghosh, S., Mehta, V.S., and Sen, E. (2012). Inhibition of casein kinase-2 induces p53-dependent cell cycle arrest and sensitizes glioblastoma cells to tumor necrosis factor (TNFα)-induced apoptosis through SIRT1 inhibition. Cell Death Dis. *3*, e271.

Doble, B.W., and Woodgett, J.R. (2003). GSK-3: tricks of the trade for a multitasking kinase. J. Cell Sci. *116*, 1175–1186.

Galli, R., Binda, E., Orfanelli, U., Cipelletti, B., Gritti, A., De Vitis, S., Fiocco, R., Foroni, C., Dimeco, F., and Vescovi, A. (2004). Isolation and characterization of tumorigenic, stem-like neural precursors from human glioblastoma. Cancer Res. *64*, 7011–7021.

García-Rodríguez, C., and Rao, A. (1998). Nuclear factor of activated T cells (NFAT)-dependent transactivation regulated by the coactivators p300/CREB-binding protein (CBP). J. Exp. Med. *187*, 2031–2036.

Hashizume, R., Ozawa, T., Dinca, E.B., Banerjee, A., Prados, M.D., James, C.D., and Gupta, N. (2010). A human brainstem glioma xenograft model enabled for bioluminescence imaging. J. Neurooncol. *96*, 151–159.

Hemmati, H.D., Nakano, I., Lazareff, J.A., Masterman-Smith, M., Geschwind, D.H., Bronner-Fraser, M., and Kornblum, H.I. (2003). Cancerous stem cells can arise from pediatric brain tumors. Proc. Natl. Acad. Sci. USA *100*, 15178–15183.

Hoeflich, K.P., Luo, J., Rubie, E.A., Tsao, M.S., Jin, O., and Woodgett, J.R. (2000). Requirement for glycogen synthase kinase-3beta in cell survival and NF-kappaB activation. Nature *406*, 86–90.

Huillard, E., Ziercher, L., Blond, O., Wong, M., Deloulme, J.C., Souchelnytskyi, S., Baudier, J., Cochet, C., and Buchou, T. (2010). Disruption of CK2beta in embryonic neural stem cells compromises proliferation and oligodendrogenesis in the mouse telencephalon. Mol. Cell. Biol. *30*, 2737–2749.

Huillard, E., Hashizume, R., Phillips, J.J., Griveau, A., Ihrie, R.A., Aoki, Y., Nicolaides, T., Perry, A., Waldman, T., McMahon, M., et al. (2012). Cooperative interactions of BRAFV600E kinase and CDKN2A locus deficiency in pediatric malignant astrocytoma as a basis for rational therapy. Proc. Natl. Acad. Sci. USA *109*, 8710–8715.

Ignatova, T.N., Kukekov, V.G., Laywell, E.D., Suslov, O.N., Vrionis, F.D., and Steindler, D.A. (2002). Human cortical glial tumors contain neural stem-like cells expressing astroglial and neuronal markers in vitro. Glia *39*, 193–206.

Kim, W.Y., Wang, X., Wu, Y., Doble, B.W., Patel, S., Woodgett, J.R., and Snider, W.D. (2009). GSK-3 is a master regulator of neural progenitor homeostasis. Nat. Neurosci. *12*, 1390–1397.

Li, R., and Botchan, M.R. (1993). The acidic transcriptional activation domains of VP16 and p53 bind the cellular replication protein A and stimulate in vitro BPV-1 DNA replication. Cell *73*, 1207–1221.

Ligon, K.L., Alberta, J.A., Kho, A.T., Weiss, J., Kwaan, M.R., Nutt, C.L., Louis, D.N., Stiles, C.D., and Rowitch, D.H. (2004). The oligodendroglial lineage marker OLIG2 is universally expressed in diffuse gliomas. J. Neuropathol. Exp. Neurol. *63*, 499–509.

Ligon, K.L., Huillard, E., Mehta, S., Kesari, S., Liu, H., Alberta, J.A., Bachoo, R.M., Kane, M., Louis, D.N., Depinho, R.A., et al. (2007). Olig2-regulated lineage-restricted pathway controls replication competence in neural stem cells and malignant glioma. Neuron *53*, 503–517.

Litchfield, D.W. (2003). Protein kinase CK2: structure, regulation and role in cellular decisions of life and death. Biochem. J. *369*, 1–15.

Lu, Q.R., Park, J.K., Noll, E., Chan, J.A., Alberta, J., Yuk, D., Alzamora, M.G., Louis, D.N., Stiles, C.D., Rowitch, D.H., and Black, P.M. (2001). Oligodendrocyte lineage genes (OLIG) as molecular markers for human glial brain tumors. Proc. Natl. Acad. Sci. USA *98*, 10851–10856.

Lu, Q.R., Sun, T., Zhu, Z., Ma, N., Garcia, M., Stiles, C.D., and Rowitch, D.H. (2002). Common developmental requirement for Olig function indicates a motor neuron/oligodendrocyte connection. Cell *109*, 75–86.

MacAulay, K., Doble, B.W., Patel, S., Hansotia, T., Sinclair, E.M., Drucker, D.J., Nagy, A., and Woodgett, J.R. (2007). Glycogen synthase kinase 3alpha-specific regulation of murine hepatic glycogen metabolism. Cell Metab. *6*, 329–337.

Marie, Y., Sanson, M., Mokhtari, K., Leuraud, P., Kujas, M., Delattre, J.Y., Poirier, J., Zalc, B., and Hoang-Xuan, K. (2001). OLIG2 as a specific marker of oligodendroglial tumour cells. Lancet *358*, 298–300.

Meggio, F., and Pinna, L.A. (2003). One-thousand-and-one substrates of protein kinase CK2? FASEB J. *17*, 349–368.

Mehta, S., Huillard, E., Kesari, S., Maire, C.L., Golebiowski, D., Harrington, E.P., Alberta, J.A., Kane, M.F., Theisen, M., Ligon, K.L., et al. (2011). The central nervous system-restricted transcription factor Olig2 opposes p53 responses to genotoxic damage in neural progenitors and malignant glioma. Cancer Cell *19*, 359–371.

Meijer, D.H., Kane, M.F., Mehta, S., Liu, H., Harrington, E., Taylor, C.M., Stiles, C.D., and Rowitch, D.H. (2012). Separated at birth? The functional and molecular divergence of OLIG1 and OLIG2. Nat. Rev. Neurosci. *13*, 819–831.

Merrick, K.A., Wohlbold, L., Zhang, C., Allen, J.J., Horiuchi, D., Huskey, N.E., Goga, A., Shokat, K.M., and Fisher, R.P. (2011). Switching Cdk2 on or off with small molecules to reveal requirements in human cell proliferation. Mol. Cell *42*, 624–636.

Nitta, R.T., Gholamin, S., Feroze, A.H., Agarwal, M., Cheshier, S.H., Mitra, S.S., and Li, G. (2015). Casein kinase 2α regulates glioblastoma brain tumor-initiating cell growth through the β-catenin pathway. Oncogene *34*, 3688–3699.

Ohnishi, A., Sawa, H., Tsuda, M., Sawamura, Y., Itoh, T., Iwasaki, Y., and Nagashima, K. (2003). Expression of the oligodendroglial lineage-associated markers Olig1 and Olig2 in different types of human gliomas. J. Neuropathol. Exp. Neurol. *62*, 1052–1059.

Patel, S., Doble, B.W., MacAulay, K., Sinclair, E.M., Drucker, D.J., and Woodgett, J.R. (2008). Tissue-specific role of glycogen synthase kinase 3beta in glucose homeostasis and insulin action. Mol. Cell. Biol. *28*, 6314–6328.

Penman, C.L., Faulkner, C., Lowis, S.P., and Kurian, K.M. (2015). Current understanding of BRAF alterations in diagnosis, prognosis, and therapeutic targeting in pediatric low-grade gliomas. Front. Oncol. *5*, 54.

Santamaría, D., Barrière, C., Cerqueira, A., Hunt, S., Tardy, C., Newton, K., Cáceres, J.F., Dubus, P., Malumbres, M., and Barbacid, M. (2007). Cdk1 is sufficient to drive the mammalian cell cycle. Nature *448*, 811–815.

Schiffman, J.D., Hodgson, J.G., VandenBerg, S.R., Flaherty, P., Polley, M.Y., Yu, M., Fisher, P.G., Rowitch, D.H., Ford, J.M., Berger, M.S., et al. (2010). Oncogenic BRAF mutation with CDKN2A inactivation is characteristic of a subset of pediatric malignant astrocytomas. Cancer Res. *70*, 512–519.

Schüller, U., Heine, V.M., Mao, J., Kho, A.T., Dillon, A.K., Han, Y.G., Huillard, E., Sun, T., Ligon, A.H., Qian, Y., et al. (2008). Acquisition of granule neuron precursor identity is a critical determinant of progenitor cell competence to form Shh-induced medulloblastoma. Cancer Cell *14*, 123–134.

Serrano, M., Lee, H., Chin, L., Cordon-Cardo, C., Beach, D., and DePinho, R.A. (1996). Role of the INK4a locus in tumor suppression and cell mortality. Cell *85*, 27–37.

Sigler, P.B. (1988). Transcriptional activation. Acid blobs and negative noodles. Nature *333*, 210–212.

Singh, S.K., Clarke, I.D., Terasaki, M., Bonn, V.E., Hawkins, C., Squire, J., and Dirks, P.B. (2003). Identification of a cancer stem cell in human brain tumors. Cancer Res. *63*, 5821–5828.

Singh, S.K., Fiorelli, R., Kupp, R., Rajan, S., Szeto, E., Lo Cascio, C., Maire, C.L., Sun, Y., Alberta, J.A., Eschbacher, J.M., et al. (2016). Post-translational modifications of OLIG2 regulate glioma invasion through the TGF-β pathway. Cell Rep. *16*, 950–966.

Sun, Y., Meijer, D.H., Alberta, J.A., Mehta, S., Kane, M.F., Tien, A.C., Fu, H., Petryniak, M.A., Potter, G.B., Liu, Z., et al. (2011). Phosphorylation state of Olig2 regulates proliferation of neural progenitors. Neuron *69*, 906–917.

Suvà, M.L., Rheinbay, E., Gillespie, S.M., Patel, A.P., Wakimoto, H., Rabkin, S.D., Riggi, N., Chi, A.S., Cahill, D.P., Nahed, B.V., et al. (2014). Reconstructing and reprogramming the tumor-propagating potential of glioblastoma stem-like cells. Cell *157*, 580–594.

Wager, T.T., Hou, X., Verhoest, P.R., and Villalobos, A. (2010). Moving beyond rules: the development of a central nervous system multiparameter optimization (CNS MPO) approach to enable alignment of druglike properties. ACS Chem. Neurosci. *1*, 435–449.

Zheng, Y., McFarland, B.C., Drygin, D., Yu, H., Bellis, S.L., Kim, H., Bredel, M., and Benveniste, E.N. (2013). Targeting protein kinase CK2 suppresses prosurvival signaling pathways and growth of glioblastoma. Clin. Cancer Res. *19*, 6484–6494.

Zhou, Q., and Anderson, D.J. (2002). The bHLH transcription factors OLIG2 and OLIG1 couple neuronal and glial subtype specification. Cell *109*, 61–73.